Chemical and structural changes in Cervus elaphus tooth enamels during fossilization (Lazaret cave): a combined IR and XRD Rietveld analysis.

Véronique Michel, Philippe Ildefonse, Guillaume Morin

Chemical and structural changes in *Cervus elaphus* tooth enamels during fossilization (Lazaret cave) : a combined IR and XRD Rietveld analysis

Corrected version

Véronique MICHEL[1], Philippe ILDEFONSE[2], Guillaume MORIN[2]

1- Institut de Paléontologie Humaine, Mus.Natn.Hist.Nat., UMR 9948 du CNRS, 1 rue René Panhard, 75013 Paris, France

2- Laboratoire de Minéralogie-Cristallographie, CNRS 09, Universités Paris 6 et 7, IPGP, 4 place Jussieu, 75252 Paris cedex 05

- Applied Geochemistry, Vol. 10, pp. 145 - 159, 1995 –
And Corrigendum Applied Geochemistry , 10, 369-371

ABSTRACT

Tooth enamel from modern and fossil (Lazaret cave) *Cervus elaphus* was characterized in order to study the chemical and structural changes during fossilization. Ca, P, Na, Mg, F, Cl, CO_3 contents were measured by chemical analyses, and infrared spectroscopy (IR) was used to determine H_2O, OH^-, PO_4^{3-} and CO_3^{2-}. Carbonate increases during fossilization and substitutes for PO_4^{3-} at the B-site and for OH at the A-site. The CO_3^{2-}-for-PO_4^{3-} substitution experiences the highest increase. H_2O and OH contents decrease during fossilization. These chemical changes may be traced by Rietveld structure refinement (XRD). Like human enamel, red deer enamel consists of apatite. A good positive correlation has been found between the a cell parameter and CO_3^{2-} contents. Refinement of atomic positions and site multiplicity allow us to describe site distortions in PO_4^{3-} polyhedra and along the 6_3 axis; these distortions are indirect probes of the substituent ions in the apatite structure.

At Lazaret cave, the karstic environment is thought to control the chemical and structural changes of the fossil enamels. Fossilization conditions have been favorable for a good conservation of the *Cervus elaphus* tooth enamels whatever their stratigraphic position and location were. These fossil enamels have experienced only slight structural and chemical changes considering their geological age. This accounts for a rapid burial in continental sediments of Lazaret prehistoric cave. These Lazaret fossil enamels could be considered as stable material which may be used for dating by the ESR and U-Th methods.

INTRODUCTION

Most investigations on biological and synthetic apatite are concerned with their crystal structure (Bonel, 1972a; Nelson and Featherstone, 1982; Doi *et al.*, 1982; Elliott *et al.*, 1985; Rey *et al.*, 1991; LeGeros 1991; Bottero *et al.*, 1992) in order to understand the formation and maturation of bone and tooth, to elucidate pathological calcifications, and to explain dental caries in human teeth.

The study of fossil bones or teeth can also provide information about the fossilization process. Paleontologists, geochronologists and geochemists (Shipman, 1981; Yokoyama *et al*., 1981; Schwarcz *et al*., 1989) are interested in this complex and exceptional processes. It is important to consider the state of preservation of fossils and their surrounding deposits in order to give an account of the taphonomy of the site. ESR dating of tooth enamel, which is considered as a stable material (Grün, 1989) in Pleistocene deposits, is mostly preferred against bone or dentine which would be more affected by the diagenesis (Grün and Schwarcz, 1987). In order to attain a better understanding of the fossilization process in calcified tissue, IR and XRD analyses should provide further information regarding the mineralogical composition of the fossil enamel, dentine and bone (Newesely, 1989; Pate *et al.*, 1989).

It is well established that inorganic phase of human tooth enamel is a carbonate-substituted hydroxyapatite (Montel, 1977; Elliott *et al*., 1985). When considering OHAp hydroxyapatite as a structural model, the formula may be written as follows:

$$\begin{array}{l} Ca_{10}\,(PO_4)_6\,(OH)_2 \\ \quad|\qquad|\qquad| \\ \quad\;\; Z\qquad B\qquad A \end{array}$$

where Z = Ca^{2+}, Na^{+}, Mg^{2+}, B = PO_4^{3-}, CO_3^{2-}, HPO_4^{2-}, and A = OH^{-}, CO_3^{2-}, F^{-}, Cl^{-}, H_2O.

In AB-type carbonate-bearing apatite, most of carbonate ions are substituted for PO_4^{3-} at B-site, while the other part replaces OH^{-} at A-site (Bonel, 1972b). The total amount of carbonate being incorporated in enamel is ~ 3 wt.%, and about 11 % were found to be at the A-site (Elliott *et al.*, 1985). Other impurities as HPO_4^{2-} are known to substitute for PO_4^{3-} in the apatite structure, while F^{-}, Cl^{-}, H_2O may be incorporated at the A-site whereas Na^{+}, Mg^{2+} replace Ca^{2+} at the Z-site (Featherstone *et al.*, 1983; LeGeros and LeGeros, 1984).

These substitutions induce changes in the properties of apatite. For example, when the carbonate content is high at the B-site, the solubility behavior of apatite increases and its crystallinity decreases (LeGeros, 1981; Doi *et al*., 1982). Sillen and LeGeros (1991) have shown that a Pleistocene fossil enamel (from Swartkrans) is less soluble than fossil bone and dentine which contain more carbonate, and is much more soluble than the fluorapatite (containing ~ 4 wt.% F^{-}).

The substituted ions induce also variations in the cell parameters of apatite. When the planar CO_3^{2-} group replaces PO_4^{3-} tetrahedron, the a lattice parameter decreases whereas c

lattice parameter slightly increases. The opposite was observed when CO_3^{2-} substitutes OH^- at the A-site (LeGeros, 1981; Nelson and Featherstone, 1982). The presence of structural H_2O at the A-site of enamel apatite (absent in stoichiometric OHAp) leads to an increase of the *a* lattice parameter (Holcomb and Young, 1980; LeGeros, 1981).

The detailed knowledge of the structural parameters of apatite constituting enamel and of their substituting ions is of prime importance in order to understand evolution of tooth enamel during fossilization. Two analytical methods are frequently used to study enamel apatites: X-ray diffraction, particularly the refinement of powder data using the Rietveld method has been used for apatite (Young and Mackie, 1980; Young and Wiles, 1981). The Rietveld method yields cell parameters with great precision and also provides indirect evidences of substituting ions. For example, the variation of scattering density along the 6_3 axis may constitute evidence of OH^- at the A-site (Young and Wiles, 1981). The second method is infrared spectroscopy which can identify unambiguously OH^- and H_2O groups at the A-site (LeGeros *et al*., 1969, 1978), and CO_3^{2-} at the A- and B-sites (Elliott *et al*., 1985).

The purpose of this study is to provide mineralogical, and crystal-chemical information on fossil enamel. In this work, modern red deer enamel is compared to fossil tooth enamels from the Lazaret prehistoric site (Nice, France). IR and Rietveld data were used to discuss the modifications of enamel during fossilization.

MATERIALS AND METHODS

Material studied

Five samples were analyzed; they consist of tooth enamel originating from adult *Cervus elaphus* mandibles. One was modern (obtained by the Anatomy laboratory, M.N.H.N., Paris) and four were fossil. The fossil mandibles come from the prehistoric cave of Lazaret (Nice, France) (Fig. 1). They were discovered in archaeological levels (Middle Pleistocene) which constitute the C continental infilling (six meters deep). These deposits have been divided into three levels : CI, CII, and CIII. They are located between a beach deposit B at the bottom and a stalagmitic flowstone E at the top. The sedimentary deposits, in a karstic environment, are characterized by a clayey gravel (de Lumley, 1976). Mandibles have been distinguished according to their stratigraphic position in the deposit (Table 1, Fig. 1).

Red deer enamel (1 mm thick) was taken from molars and was separated from dentine with a dentist's drill. Enamel specimens were reduced to powder at a size < 50 μm in an agate mortar. All samples investigated consist only of apatite.

Methods

Chemical analysis

Electron microprobe analysis of enamel were done on a Camebax instrument (15 Kv, 10 nA) equipped with WDS on polished sections (teeth were embedded in an acrylic resin under vacuum). Measurements of Ca, P, Na, Mg, Cl contents were obtained by comparison with a known standard (fluorapatite from Durango, Mexico). The amounts (wt.%) correspond to an average of forty analyses on each specimen (Table 1). The CO_3 contents were determined by a coulometric titration of the CO_2 released from an acidified aqueous solution of the powdered samples (± 0.01%) and the F contents by specific ion-meter (± 20 ppm) by the X-Ral laboratory (Canada).

Infrared spectrometry

A standard procedure was used for sample preparation (Fröhlich, 1989). 20 mg of the powered enamel (size < 20 µm) were ground under acetone with agate balls in an agate mortar placed in a refrigerated area (4°C). Grinding time of one hour was done to obtain a particle size less than 5 µm. The KBr pellets were prepared by mixing 7.5 mg of enamel with 300 mg of KBr. After drying the mixture at 80°C over one night, a 300 mg transparent pellet (13 mm in diameter) was made under vacuum and under a pressure of 11 ton.cm^{-2}.The IR spectra were recorded in transmittance mode with a Perkin Elmer 16 FPC-FTIR spectrometer.

Three regions of interest were selected: 1760-1320 cm^{-1}, 900-830 cm^{-1}, and 740-490 cm^{-1}. In order to quantify the CO_3^{2-} and PO_4^{3-}, the envelopes were decomposed into Lorentzian components according to the number and the positions of identified absorption bands. The calculated positions of individual bands are the same (± 1 cm^{-1}) for all samples. Experimental and calculated spectra were fitted by least squares procedure. The band areas were calculated by least squares procedure.

X-ray diffraction and Rietveld analysis

Enamel samples were mixed with an internal standard NaF (10 wt.%) and ground (size < 20 µm) under acetone in an agate mortar. The X-ray powder data were collected on an automated Siemens D501 diffractometer, equipped with a graphite monochromator and operating in step scan mode using CuKα radiation. X-ray data were collected between 30 and 140° 2Θ with a 0.04° 2Θ step and counting 40s by step.

Rietveld refinements were done with the XND code (Berar, 1990). The refined values (a and c cell parameters, atomic positions, site occupancies, thermal parameters) of stoichiometric OHAp (Sudarsanan and Young, 1969) were used as the starting model (Young and Mackie, 1980). The Voigt function was used to represent the individual reflection profiles, allowing us to deconvolute the strain and the size broadening contributions (Howard

and Preston, 1989). In the final step of the refinement, all atomic positions and site occupancies were refined simultaneously, with atom displacement factors fixed at single-crystal values (Sudarsanan and Young, 1969).

RESULTS AND DISCUSSION

Chemical data

The atomic ratio Ca/P of stoichiometric OHAp, Ca_{10} $(PO_4)_6$ $(OH)_2$ is 1.67. The Ca/P of samples studied, calculated from microprobe analysis (Table 1) range between 1.60 and 1.67. The same range of Ca/P values (1.59-1.66) was found in human enamel (Bottero *et al*., 1992). The CO_3 content (4.13%) of modern enamel is slightly lower than that of fossil enamels (4.60-4.94%) but is not clearly correlated to the stratigraphic position of the teeth studied. The Ca'/P values (where Ca'= Ca+Na+Mg) do not change significantly among the samples. The fluorine contents of the fossil enamel samples are very small (< 0.1%). L80 sample is considered as the oldest fossil studied, due to its stratigraphic position; it contains 146 ppm of fluorine, essentially the same as that measured (136 ppm) in enamel of the modern red deer (Table 1).

Modern and fossil enamels are chemically homogeneous regardless of the age of the teeth. The red deer enamel has a chemical composition close to that reported for human enamel (Driessens, 1980; LeGeros and LeGeros, 1984).

The low amount of fluorine can be rationalized by the karstic environment which prevails in the Lazaret cave. The clayey matrix which contained the mandibles was rich in calcite and quartz. A stalagmitic flowstone is forming in the cave, and the slightly basic ground water (pH = 7.96) is saturated with respect to calcium carbonate which precipitates as calcite.

Infrared data

Infrared spectra of modern and fossil *Cervus elaphus* enamels have the same characteristic absorption bands as the IR spectra of synthetic apatites containing CO_3 at both A- and B-sites (Bonel, 1972b) and of modern human enamel (Holcomb and Young, 1980 ; Elliott *et al*., 1985). The IR bands for fossil and modern enamels have been related to PO_4 group, CO_3 groups at the A-and B-sites, and to H_2O and OH according to literature (Holcomb and Young, 1980; LeGeros, 1981; Young *et al.*, 1981; Rey *et al*., 1991) (Table 2, Fig. 2).

The most significant change in IR spectra of modern and fossil enamels concerns the large H_2O bands which mask the OH stretching band at 3567 cm^{-1} (Fig. 2). The amplitude of

the H_2O stretching and bending bands at 3430-3300 cm^{-1} and 1650 cm^{-1} respectively is higher in modern enamel than in the fossil samples (Fig. 2A). Fossil enamels have lost most of their organic matter and as a consequence contain less adsorbed (3430 cm^{-1} band) and structural H_2O (3330 cm^{-1} band, Holcomb and Young, 1980) than modern enamel. The OH bending band at 630 cm^{-1} in the synthetic hydroxyapatite and enamel IR spectra (Nelson and Featherstone, 1982; Rey *et al.*, 1991) appears only as a shoulder on the left side of the ν_4 PO_4^{3-} band on the fossil and modern enamels (Fig. 3).

Quantification of the PO_4 and CO_3 groups: two examples (modern and L80 fossil enamels) of the decomposition procedure of complex IR bands into component bands are presented in Figs. 2B, 3, 4 and 5. This procedure allows an estimation of the amount of PO_4^{3-} and CO_3^{2-} groups in enamels studied. The position and area of individual bands for all enamels are listed in Table 3.

740-490 cm^{-1} region: there are four bands in this region (Fig. 3). Three are related to PO_4^{3-} groups (605, 576, 565 cm^{-1}) and the fourth one to OH^- (630 cm^{-1}). This last one is slightly higher in amplitude in modern enamel than in fossil enamels (Table 3). In the following text, the amount of PO_4^{3-} will be determined by the area of the 565 cm^{-1} component.

1760-1320 cm^{-1} region: the broad band encountered in this region has been decomposed in seven Lorentzian components (Fig. 4). Five bands (1548, 1501, 1470, 1451 and 1412 cm^{-1}) are related to CO_3^{2-} groups and two bands (1620-1640 and 1661-1669 cm^{-1}) to H_2O and organic matter (Table 3). As mentioned before, the relative intensities of these two last bands decrease significantly in the fossil enamels with respect to the modern enamel. Amounts of CO_3^{2-} at the A- and B-sites have been estimated by the area under the Lorentzian curves around 1548 and 1412 cm^{-1} respectively. The B-CO_3^{2-}/PO_4^{3-} ratios are higher in fossil enamels than in modern enamel. The opposite is observed for the A-CO_3^{2-} area. These data suggest that CO_3^{2-} occurs primarily at the B-site of apatite in fossil enamel.

900-830 cm^{-1} region: the broad band may be decomposed in three Lorentzian components at 965, 872, 880 cm^{-1} (Fig. 5). These bands are due to three CO_3^{2-} groups: A-CO_3^{2-} (880 cm^{-1}), B-CO_3^{2-} (872 cm^{-1}) and a third CO_3^{2-} group (865 cm^{-1}) which has not been actually attributed to a specific site (Rey *et al.*, 1991). HPO_4^{2-} could be also a candidate for the 872 cm^{-1} band (Holcomb and Young, 1980), but it cannot be distinguished from the CO_3^{2-} group at the same wavenumbers unless the samples were ignited. This is the reason why we used the 1412 cm^{-1} band to assess the CO_3^{2-} content at the B-site. Nevertheless, the A-CO_3^{2-}/B-CO_3^{2-} area ratios measured both with 879 -873 cm^{-1} or 1547-1412 cm^{-1} bands are higher in modern enamel than that in fossil enamel (Table 3). These data imply that during fossilization, CO_3^{2-} is preferentially incorporated at the B-site as yet mentioned through the CO_3^{2-} band at 1412 cm^{-1}. The area of the third CO_3^{2-} band is the same in all the samples studied.

Rietveld refinements

Two examples of Rietveld refinements (modern and L80 enamels) are presented in Fig. 6. Refined structural parameters obtained for all enamels studied are reported in Tables 4 and 5. Rwp, Rp and R-Bragg agreement indices for Rietveld refinements (Post and Bish, 1989) indicate the quality of the fits.

Cell parameters: Cell parameters of all enamels studied are slightly higher than those of the OHAp refined by Sudarsanan and Young (1969) (Table 4) and are similar to values reported for human enamel (Fig. 7A) (Young and Mackie, 1980, Bottero *et al.*, 1992).
The a parameter is ~0.02 Å higher than in OHAp. It is highest in modern red deer enamel (9.4468 Å) and is slightly lower in fossil ones (9.4396-9.4444 Å) (Fig. 7B). Besides, in fossil enamels studied here, there is a negative correlation (r=0.92) between the a parameter and the CO_3^{2-} content (Fig. 7B) suggesting that CO_3^{2-} groups replace PO_4^{3-} ions in the apatite structure. An increase of the a parameter has been correlated with the presence of structurally incorporated H_2O at the A-site in an "aqueous" synthetic OH-apatite (a=9.438 Å; LeGeros, 1981). When their samples were heated past to 400°C the a parameters return to normal OHAp a value. In human or red deer enamel apatite, the situation is more complex because both H_2O and CO_3^{2-} incorporate the apatite structure. a parameter decreases with increasing CO_3^{2-} content both in "high temperature" (Nelson and Featherstone, 1982) and "aqueous" synthetic apatites (Nelson and Featherstone, 1982; Okazaki, 1983) (Fig. 7A). But, "aqueous" apatites, human and red deer enamels are characterized by a higher a value than OH-apatite and "high temperature" carbonated-apatites at low CO_3^{2-} content (<5%). This higher a value is due to structurally incorporated H_2O.
The c parameter (6.8861-6.8880 Å) does not change significantly in the samples studied (Fig. 7B). In synthetic apatites, a contraction in the a and an expansion in the c parameters with increasing CO_3^{2-} contents were measured. Besides, sodium incorporation occurs together with the carbonate substitution in order to respect the electroneutrality in the apatite structure (LeGeros, 1981; Nelson and Fearthertone, 1982). The increase of the c lattice parameter was not observed for the red deer enamels studied here. Moreover, the sodium contents of fossil enamels increase with the CO_3^{2-} contents and the Mg content remains constant (Table 1).

Substitutions at the A- and B-sites:

Background: we expected that incorporation of other species may be detected by looking at local distortions. Thus, when CO_3^{2-} replaces PO_4^{3-} at the B-site, the atomic positions must differ from those in stoichiometric OHAp (Young and Wiles, 1981). Furthermore, H_2O, CO_3^{2-}, Cl^- and F^- which substitute for OH^- at the A-site change

distribution of the scattering density along the 6_3 axis (Young and Mackie, 1980; Young and Wiles, 1981; Young and Holcomb, 1982). Two refinements were made with dummy oxygen atoms placed at (1) 0,0, z = 0, 0.10, 0.20; (2) 0,0, z = 0.05, 0.15, 0.25, and the site occupancy for each dummy oxygen was refined. This procedure yields a representation of the distribution of scattering density along the channels centered on the 6_3 axis. The scattering density in OHAp, measured from neutron data, has a maximum at z = 0.20, corresponding to the oxygen coordinates (z=0.1978) and another smaller which is related to the hydrogen's position (z=0.0608) (Young and Wiles, 1981). By comparison of the neutron and X-ray data, Young *et al.*, (1981) estimated the position parameters (0,0,z = 0.12) of the A-site occupied by CO_3^{2-} in human enamel. According to Young and Wiles (1981), H_2O seems to be localized at 0,0,z = 0.12-0.14 and Cl^- at 0,0,z = 0.06-0.08. The distribution of scattering density in human enamel shows a new maximum at 0,0,z = 0.10-0.15, and confirms the presence of H_2O and CO_3^{2-} at the A-site. The same procedure was applied on the *Cervus elaphus* enamels studied here.

Indirect evidence of (CO_3^{2-}, H_2O)-for-OH^- substitution at the A-site in Cervus elaphus enamels: the distribution of scattering density along the channels are shown in Tables 4, 5 and Fig. 8. E1334 and F72 enamels have a maximum density at 0,0,z = 0.15. For the three other enamels studied, there are maxima at 0,0,z = 0.15 and z = 0.20 (Fig. 8). The 0.15-value departs from the z=0.20 value reported for OH^- in stoichiometric OHAp, and is close to the value refined for human enamel (Young and Mackie, 1980). This is interpreted as a signature of H_2O and CO_3^{2-} substituting for OH^- at the A-site.

Indirect evidence of CO_3^{2-}-for-PO_4^{3-} substitution in B site in Cervus elaphus enamels: P-O(3) distances in all enamels studied (1.428-1.500 Å) are shorter than that in stoichiometric OHAp (1.529 Å), and fossil enamels yield the shortest distances (Table 6). On the other hand, P-O(2) distances are larger in *Cervus elaphus* enamels (1.561-1.587Å) than in OHAp (1.545Å) and the difference larger in fossil enamels. The P-O(1) distances are also shorter in *Cervus elaphus* enamels (1.492-1.517 Å) than in OHAp (1.537 Å) but do not change significantly among the enamels studied.

Comparison of respective amounts of CO_3^{2-} at the A- and B-sites derived from IR spectrometry and the refined P-O(2) and P-O(3) distances are presented in Fig. 9. There are good correlation between the decrease of the P-O(3) distance (r=0.88) and P-O(2) distances (r=0.93) with the amount of CO_3^{2-} at the B-site. This comparison indicates that the planar CO_3^{2-} ion substitutes for the PO_4^{3-} tetrahedron at the B-site and that this substitution induces local distortions in *Cervus elaphus* tooth enamels.

***Crystallinity and order-disorder*:** Line profile analysis was done by using Voigt function which allows to deconvolute the strain and the size broadening contributions (Howard and Preston, 1989). Integral breath of the Lorentzian function is related to mean

coherent domain size and integral breath of the Gaussian function is due to structural disorder. Three Lorentzian functions were used along a, b and c directions of the apatite structure which give access to three integral breath Wla, Wlb and Wlc. Besides, Wg yields an estimation of the strain or structural disorder (Table 7). Derived mean coherent domain size by using Sherrer formula range from 466 to 505 Å, from 488 to 619 Å and from 470 to 535 Å along a, b, and c direction respectively. No significant MCD shape anisotropy was observed. MCD a and MCD b decrease in fossil enamels according to their stratigraphic position in the deposits, L80 enamel, the oldest one having the smallest values (Figs. 10A, 10B). The structural disorder measured by the Wg value increases as the a parameter decreases (r= 0.87) (Fig. 11). This behavior could be related to the substituent ions and molecules in the apatite structure and the best correlation was found with the CO_3^{2-} at the A-site (Fig. 11). Wg is thus a sensitive probe of defect structure due to substitutional impurities in the apatite structure whereas MCD b / MCD a ratio is inversely correlated to the age of the enamel studied. Besides, the increased crystallinity represented by the MCD b / MCD a ratio may be related to the increasing fluorine content (Fig. 10C). This relationship has been previously reported for synthetic apatites where fluorine promotes crystal growth (LeGeros, 1981). The youngest E1334 fossil enamel with the highest fluorine content has a larger crystal size than that in the oldest L80 fossil enamel. Therefore, the crystallinity distribution profile suggests that a slight post-depositional alteration of fossil enamels took place in the lower levels of the continental deposits (Fig. 10).

State of preservation of fossil enamels and their geological environment

The type and the state of preservation of enamels contribute to describe post-mortem history and therefore to reveal changes in geochemical surrounding conditions. The deposits, where fossils have been excavated, inevitably control their preservation state. At Lazaret cave, the clayey sediments, loaded by stream carbonate saturated water, is a moderately alkaline environment. Fossilization conditions have been favorable for a good conservation of the tooth enamels whatever their stratigraphic position and location were. These fossil enamels experienced only slight structural and chemical changes considering their geological age (Middle Pleistocene). This accounts for a rapid burial in continental sediments at Lazaret prehistoric cave in agreement with the exceptional amount of excavated mammal remains (artiodactyls and carnivores >70 000) (Valensi, 1994).

CONCLUSION

Cervus elaphus enamels consist of finely divided apatite-like crystals which incorporate CO_3^{2-}, H_2O and Na^+. Their crystallographic characters are similar to that of human enamel. IR spectroscopy and Rietveld refinement show that CO_3^{2-} substitutes for PO_4^{3-} and OH^-, and that B-site contains the highest amount of CO_3^{2-}. Fossil enamels may be distinguished from modern red deer enamel by their highest carbonate and lowest H_2O contents. Loss of adsorbed H_2O during fossilization is mainly related to the decay of organic matter constituting modern enamel. Carbonation in the B-site induces a decrease of the a cell parameter of the fossil enamels with respect to the modern enamel. Carbonation of the apatite is interpreted as a consequence of the geological environment which prevails during and after the fossilization.

Characterization of the mineralogical constituents of teeth or bones, which are frequently used for dating prehistoric sites, has to be accurately done by combining methods such as infrared spectroscopy and Rietveld structure refinement using powder X-ray diffraction data. Moreover, the knowledge of chemical and structural changes during fossilization is of prime importance for a better confidence in dating. Further investigation of the enamel suitability for ESR dating are in progress (Michel, 1995).

Acknowledgments - Authors are indebted to Dr. J-D. Vigne and Prof. H. de Lumley for supplying the modern red deer mandible and the fossil *Cervus elaphus* mandibles respectively. Authors would like to thank Dr. F. Fröhlich for the help in the IR and XRD acquisitions and for his comments. This paper benefited of thoughtful and constructive reviews by Prof. H.P. Schwarcz, and two anonymous reviewers. This study has been supported by IPGP/xxxx (Ph. I.)

REFERENCES

Bérar J-F. (1990) Reduction of the number of parameters in real time Rietveld refinements. I.U.Cr. Sat. Meeting Powder Diffraction, Toulouse.

Bonel G. (1972a) Contribution à l'étude de la carbonatation des apatites. I. - Synthèse et étude des propriétés physico-chimiques des apatites carbonatées du type A. *Ann. Chim.* **7**, 65-88.

Bonel G. (1972b) Contribution à l'étude de la carbonatation des apatites. II.- Synthèse et étude des propriétés physico-chimiques des apatites carbonatées du type B. III.- Synthèse et étude des propriétés physico-chimiques des apatites carbonatées dans deux types de sites. Evolution des spectres infrarouge en fonction de la composition des apatites. *Ann. Chim.***7**, 127-144.

Bottero M.J., Yvon J. and Vadot J. (1992) Multimethod analysis of apatites in sound human tooth enamel. *Eur. J. Mineral.* **4**, 1347-1357.

Doi Y., Moriwaki Y., Aoba T., Takahasshi J. and Joshin K. (1982) ESR and IR studies of carbonate-containing hydroxyapatites. *Calcif. Tissue Int.* **34**, 178-181.

Driessens F.C.M. (1980) The mineral in bone, dentin and tooth enamel. *Bull. Soc. Chim. Belg.* **89**, 663-687.

Elliott J.C., Holcomb D.W. and Young R.A. (1985) Infrared determination of degree of substitution of hydroxyl by carbonate ions in human dental enamel. *Calcif. Tissue Int.* **37**, 372-375.

Featherstone J.D.B., Mayer I., Driessens F.C.M., Verbeeck R.M.H. and Heijligers H.J.M. (1983) Synthetic apatites containing Na, Mg and CO_3 and their comparison with tooth enamel mineral. *Calcif. Tissue Int.* **35**, 169-171.

Fröhlich F. (1989) Deep-sea biogenic silica : new structural and analytical data from infrared analysis - geological implications. *Terra Nova* **1**, 267-273.

Grün R. (1989) Electron spin resonance (ESR) dating. *Quaternary Internat.* **1**, 65-109.

Grün R. and Schwarcz H. (1987) Some remarks on "ESR dating of bones". *Ancient TL* **5**, 1-9.

Holcomb D.W. and Young R.A. (1980) Thermal decomposition of tooth enamel. *Calcif. Tissue Int.* **31**, 189-201.

Howard S.A. and Preston K.D. (1989) Profile fitting of powder diffraction patterns. In *Modern Powder Diffraction* (eds D.L. Bish and J.E. Post), Reviews in Mineralogy, Vol. 20, Chap. 8, pp. 217-275. Mineralogical Society of America.

LeGeros, R.Z., Trautz, O.R., Klein, E., and LeGeros, J.P. (1969) Two types of carbonate substitution in the apatite structure. *Experientia* **24** , 5-7.

LeGeros, R.Z., Bonel, G., and Legros, R. (1978) Types of H_2O in human enamel and in precipitated apatites. *Calcif. Tissue Res*. **26**, 111-118.

LeGeros R.Z. (1981) Apatites in biological systems. *Prog. Crystal Growth Charact*. **4**, 1-45.

LeGeros R.Z. and LeGeros J.P. (1984) Phosphate minerals in human tissues. In *Phosphate minerals* (eds J.O. Nriagu and P.B. Moore), Chap. 12, pp. 351-385. Springer-Verlag, Berlin.

LeGeros R.Z. (1991) Magnesium in normal and pathological calcifications. In *Mechanisms and phylogeny of mineralization in biological systems* (eds S. Suga and H. Nakahara), Chap. 3.6, pp. 315-319. Springer-Verlag, Tokyo.

Lumley H. de (1976) Grotte du Lazaret. In *Sites paléolithiques de la Région de Nice et grottes de Grimaldi*, IXth U.I.S.P.P. Meeting, Nice, France, **B1**, pp. 53-75.

Michel V. (1995) Datation du remplissage continental de la grotte du Lazaret par les méthodes ESR et U-Th appliquées à l'émail, dentine et os de *Cervus elaphus*. PhD Thesis, Mus. Natn. Hist. Nat., Paris (in preparation).

Montel G. (1977) Constitutions et structures des apatites biologiques: influence de ces facteurs sur leurs propriétés. *Biol. Cell.* **28**, 179-186.

Nelson D.G.A. and Featherstone J.D.B. (1982) Preparation, analysis, and characterization of carbonated apatites. *Calcif. Tissue Int.* **34**, S69-S81.

Newesely H. (1989) Fossil bone apatite. *Appl. Geochem.* **4**, 233-245.

Okazaki M. (1983) F^--CO_3^{2-} interaction in IR spectra of fluoridated CO_3 apatites. *Calcif. Tissue Int.* **35**, 78-81.

Pate F. D., Hutton J. T. and Norrish K. (1989) Ionic exchange between soil solution and bone : toward a predictive model. *Appl. Geochem.* **4**, 303-316.

Post J.E. and Bish D.L. (1989) Rietveld refinement of crystal structures using powder X-ray diffraction data. In *Modern Powder Diffraction* (eds D.L. Bish and J.E. Post), Reviews in Mineralogy, Vol. 20, Chap. 9, pp. 277-308. Mineralogical Society of America.

Rey C., Renugopalakrishnan V., Shimizu M., Collins B. and Glimcher M. J. (1991) A resolution-enhanced Fourier transform spectroscopic study of the environment of the CO_3^{2-} ion in the mineral phase of enamel during its formation and maturation. *Calcif. Tissue Int.* **49**, 259-268.

Schwarcz H. P., Hedges R. E. M. and Ivanovich M. (1989) Editorial comments on the first international workshop on fossil bone. *Appl. Geochem.* **4**, 211-213.

Shipman P. (1981) *Life history of a fossil. An introduction to taphonomy and paleoecology.* Harvard University Press, Cambrige, England.

Sillen A. and LeGeros R. (1991) Solubility profiles of synthetic apatites and of modern and fossil bones. *J. of Archaeol. Sci.* 1**8**, 385-397.

Sudarsanan K. and Young R.A. (1969) Significant precision in crystal structural details : Holly Springs hydroxyapatite. *Acta Cryst.* **B25**, 1534-1543.

Valensi P. (1994) Les grands mammifères de la grotte du Lazaret, Nice. Etude paléontologique et biostratigraphique des carnivores. Archéozoologie des grandes faunes. PhD Thesis, Mus. Natn. Hist. Nat., Paris, 500 p.

Yokoyama Y., Quaegebeur J. P., Bibron R., Leger C., Nguyen H.V. et Poupeau G. (1981) Electron spin resonance (ESR) dating of bones of the Caune de l'Arago at Tautavel. In *Absolute dating and isotope analysis in prehistory - methods and limits* (eds. H. de Lumley and J. Labeyrie), pp. 457-492. Proceeding.

Young R.A. and Mackie P.E. (1980) Crystallography of human tooth enamel : Initial structure refinement. *Mat. Res. Bull.* **15**, 17-29.

Young R.A. and Wiles D.B. (1981) Application of the Rietveld method for structure refinement with powder diffraction data. *Adv. X-ray Anal.* **24**, 1-23.

Young R.A., Bartlett M.L., Spooner S., Mackie P.E. and Bonel G. (1981) Reversible high temperature exchange of carbonate and hydroxyl ions in tooth enamel and synthetic hydroxyapatite. *J. Biol. Phys.* **9**, 1-34.

Young R.A. and Holcomb D.W. (1982) Variability of hydroxyapatite preparations. *Calcif. Tissue Int.* **34**, S17-S32.

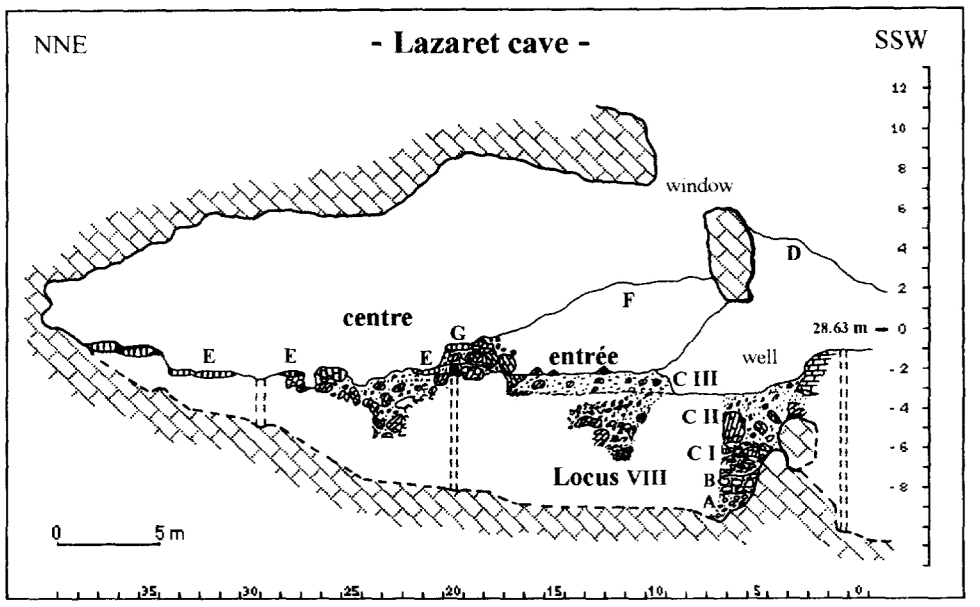

Fig. 1. Synthetic longitudinal section of Lazaret cave (modified from de Lumley, 1976).

Table 1. Stratigraphic position and chemical composition of modern and fossil red deer enamels

Z (cm)	Level	Sample	Ca	P	Na	Mg	Cl	CO_3	F	Ca/P	Ca′/P
—	—	Modern red deer	37.85	18.12	0.47	0.12	0.37	4.13	136	1.61	1.66
−317	CIII	*E1334	39.28	18.45	0.50	0.12	0.30	4.83	950	1.64	1.69
−362	CII	*F72	37.40	17.82	0.43	0.13	0.28	4.60	950	1.62	1.66
−435	CII	*L23	38.63	17.90	0.58	0.12	0.28	4.94	418	1.67	1.72
−660	CI	*L80	38.82	18.62	0.48	0.13	0.32	4.84	146	1.61	1.65

The stratigraphic reference plane (Z = 0 cm) corresponds to +28.63 m above sea level. The excavation area is indicated as *: E, fouille entrée; F, fouille centre; L, Locus VIII. The Ca, P, Na, Mg and Cl contents were determined by microprobe analysis (wt.%). CO_3 was analyzed by coulometry (±0.01 wt.%). F was analyzed by fluorine specific ion electrode (±20 ppm). Ca/P, Ca′/P are calculated molar ratios; Ca′ = Ca + Na + Mg.

Table 2. Observed infrared band-positions (cm^{-1}) of modern enamel and fossil red deer enamels from Lazaret cave.

IR absorption bands	positions
OH	3567 (w)
H_2O	3300–3430 (s)
H_2O—organic	~1650 (*)
carbonate ν_3	1545 (w)
	1500 (w)
	1470 (w)
	1456 (s)
	1415 (s)
Phosphate ν_3	1090 (vs)
	1040 (vs)
Phosphate ν_1	961 (m)
Carbonate ν_2	879 (m)
	873 (m)
OH	630 (w)
Phosphate ν_4	604 (vs)
	575 (s)
	565 (vs)
Phosphate ν_2	472 (w)

Band intensities are designated by (vs) = very strong; (s) = strong; (m) = medium; (w) = weak. The IR band at ~1650 cm^{-1} (*) is very strong for modern enamel and weak for fossil enamels; band positions are accurate to ±1 cm^{-1}

Table 3. Positions, areas and area ratios of resolved IR bands of modern and fossil enamels

Bands		Modern		E1334		F72		L23		L80	
		cm^{-1}	area	cm^{-1}	area	cm^{-1}	area	cm^{-1}	area	cm^{-1}	area
		565	11.07	563.5	10.21	563.5	10.58	563	9.37	563.5	10.31
ν_4 PO_4		576	6.65	576	6.81	576	6.92	575.5	5.84	576	6.34
		605.5	10.51	605	9.86	605	9.82	605	8.62	605	9.60
OH		630	3.46	630	3.56	630	4.02	630	3.68	630	3.60
		865.5	0.39	865	0.40	865	0.41	864.5	0.37	865	0.40
ν_2 CO_3	B	873	0.52	872.5	0.53	872.5	0.54	872	0.47	872.5	0.54
	A	880	0.31	879	0.27	879.5	0.27	879	0.23	879.5	0.28
	B	1412.5	7.05	1412.5	6.76	1412.5	7.33	1412.5	6.08	1412.5	6.85
		1451	6.18	1451	5.58	1452.5	6.33	1452	5.56	1451.5	5.82
ν_3 CO_3		1470	4.99	1471	5.15	1472.5	4.42	1472.5	3.98	1471.5	4.95
		1501	2.56	1500.5	3.22	1501	3.37	1501.5	2.96	1500.5	3.02
	A	1547	4.92	1548	2.96	1548.5	3.20	1548.5	2.97	1548.5	2.78
H_2O and organic matter		1639	5.08	1628	1.35	1625	1.74	1623.5	1.66	1623.5	1.15
		1669	3.04	1669	0.59	1661.5	0.81	1663	0.53	1662	0.88

Area ratios	Modern	E1334	F72	L23	L80
A(879)/B(873)	0.605	0.504	0.497	0.485	0.511
A(1547)/B(1412)	0.698	0.438	0.437	0.488	0.406
B(1412)/PO_4(565)	0.637	0.662	0.693	0.649	0.664
B(873)/PO_4(565)	0.047	0.052	0.051	0.050	0.052

Table 4. Rietveld refinement results of fossil and modern red deer enamels with oxygens placed at 0,0, z = 0; 0.10; 0.20

Red deer enamels		Modern	E1334	F72	L23	L80	OHAp+
Ca(1)	z	−0.0009(7)	0.0005(8)	0.0002(8)	−0.0006(7)	−0.0006(7)	0.0013(1)
	n	0.323(4)	0.324(4)	0.312(4)	0.317(4)	0.314(4)	0.3333
Ca(2)	x	0.2482(3)	0.2452(4)	0.2459(4)	0.2476(4)	0.2479(3)	0.2465(1)
	y	0.9889(4)	0.9871(4)	0.9878(5)	0.9886(4)	0.9895(4)	0.9931(1)
	n	0.472(6)	0.470(6)	0.446(6)	0.463(6)	0.458(5)	0.5
P	x	0.3981(4)	0.3955(5)	0.3963(5)	0.3976(4)	0.3969(4)	0.3983(1)
	y	0.3681(4)	0.3665(5)	0.3666(5)	0.3672(4)	0.3669(4)	0.3683(1)
	n	0.447(5)	0.439(6)	0.419(6)	0.436(6)	0.442(5)	0.5
O(1)	x	0.3324(7)	0.3359(9)	0.3323(9)	0.3333(8)	0.3333(7)	0.3282(2)
	y	0.4845(8)	0.486(1)	0.485(1)	0.4857(9)	0.4855(8)	0.4846(1)
	n	0.56(1)	0.49(1)	0.54(1)	0.54(1)	0.54(1)	0.5
O(2)	x	0.5888(8)	0.5866(8)	0.5897(9)	0.5891(8)	0.5897(7)	0.5876(1)
	y	0.4707(9)	0.4756(9)	0.477(1)	0.4716(9)	0.4722(8)	0.4652(1)
	n	0.52(1)	0.54(1)	0.50(1)	0.52(1)	0.520(9)	0.5
O(3)	x	0.3448(3)	0.3398(7)	0.3426(8)	0.3450(7)	0.3450(6)	0.3433(1)
	y	0.2661(7)	0.2658(7)	0.2674(8)	0.2664(7)	0.2673(6)	0.2579(1)
	z	0.069(1)	0.078(1)	0.079(1)	0.069(1)	0.072(1)	0.0704
O(H)(1)	z*	0	0	0	0	0	0.1978(7)
	n1	0.016(7)	−0.025(8)	−0.043(9)	0.010(7)	0.006(6)	0.3333
O(H)(2)	z*	0.10	0.10	0.10	0.10	0.10	
	n2	0.11(1)	0.10(1)	0.16(1)	0.12(1)	0.141(9)	
O(H)(3)	z*	0.20	0.20	0.20	0.20	0.20	
	n3	0.172(7)	0.120(6)	0.141(8)	0.166(6)	0.176(6)	
a (Å)		9.4468(2)	9.4396(2)	9.4444(3)	9.4422(3)	9.4410(2)	9.424(4)
c (Å)		6.8880(2)	6.8887(2)	6.8861(3)	6.8865(2)	6.8871(2)	6.879(4)
γ (°)		120.022	120.014	120.019	120.019	120.003	120
Rwp		0.0804	0.0895	0.1041	0.0854	0.0805	
Rp		0.0635	0.0703	0.0742	0.0668	0.0589	
R-Bragg		0.079	0.078	0.083	0.084	0.068	

The positional coordinates and thermal parameters of OHAp were used as the starting model (+Sudarsanan and Young, 1969). Numbers in brackets are standard deviations at the last digit.
*Fixed value.

Table 5. Rietveld refinement results of fossil and modern red deer enamels with oxygens placed at 0,0, z = 0.05; 0.15; 0.25

Red deer enamels		Modern	E1334	F72	L23	L80
Ca(1)	z	−0.0009(7)	0.0007(7)	0.0006(9)	−0.0006(7)	−0.0007(7)
	n	0.323(4)	0.327(4)	0.313(5)	0.316(4)	0.312(4)
Ca(2)	x	0.2483(3)	0.2451(4)	0.2460(4)	0.2478(4)	0.2482(3)
	y	0.9889(4)	0.9870(4)	0.9880(5)	0.9888(4)	0.9896(4)
	n	0.471(5)	0.471(6)	0.446(6)	0.463(6)	0.456(5)
P	x	0.3982(4)	0.3956(5)	0.3963(5)	0.3977(4)	0.3970(4)
	y	0.3683(4)	0.3668(5)	0.3667(5)	0.3674(4)	0.3668(4)
	n	0.447(5)	0.440(6)	0.417(6)	0.438(6)	0.439(5)
O(1)	x	0.3324(7)	0.3354(9)	0.3325(9)	0.3333(8)	0.3331(7)
	y	0.4854(8)	0.486(1)	0.485(1)	0.4861(9)	0.4852(8)
	n	0.56(1)	0.50(1)	0.54(1)	0.54(1)	0.54(2)
O(2)	x	0.5888(8)	0.5868(8)	0.5896(9)	0.5893(8)	0.5897(8)
	y	0.4706(9)	0.4762(9)	0.478(1)	0.4716(9)	0.4717(9)
	n	0.53(1)	0.54(1)	0.50(1)	0.53(1)	0.52(1)
O(3)	x	0.3451(7)	0.3396(8)	0.3424(9)	0.3456(7)	0.3452(7)
	y	0.2663(6)	0.2658(8)	0.2672(8)	0.2668(7)	0.2671(7)
	z	0.069(1)	0.079(1)	0.080(1)	0.069(1)	0.070(1)
O(H)(1)	z*	0.05	0.05	0.05	0.05	0.05
	n1	0.056(6)	−0.004(6)	−0.000(8)	0.060(6)	0.030(6)
O(H)(2)	z*	0.15	0.15	0.15	0.15	0.15
	n2	0.14(1)	0.13(1)	0.20(1)	0.15(1)	0.18(1)
O(H)(3)	z*	0.25	0.25	0.25	0.25	0.25
	n3	0.103(7)	0.064(6)	0.056(9)	0.103(7)	0.114(6)
Rwp		0.0804	0.0895	0.1051	0.0854	0.0805
Rp		0.0639	0.0707	0.0752	0.0670	0.0635
R-Bragg		0.078	0.078	0.085	0.083	0.074

Numbers in brackets are standard deviations at the last digit.
*Fixed value.

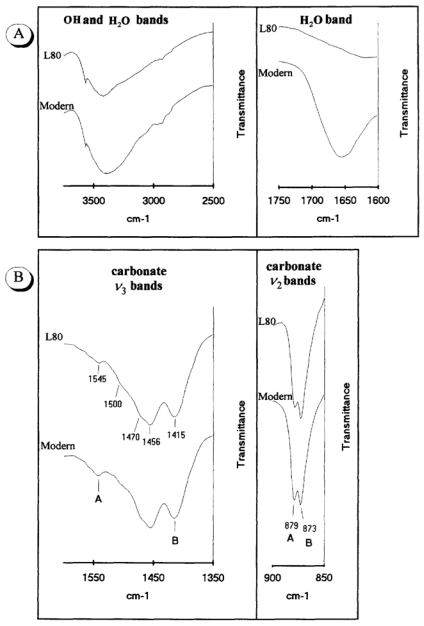

Fig. 2. IR spectra of enamels. (A) H_2O and OH bands of the modern red deer (bottom) and L80 fossil (top). (B) Carbonate bands of modern red deer (bottom) and L80 fossil (top).

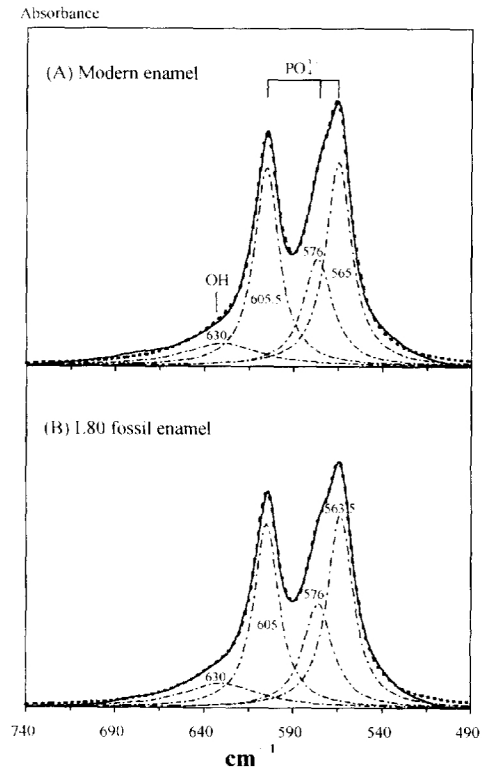

Fig. 3. OH and ν_4 PO_4^{3-} bands of (A) the modern red deer enamel and (B) L80 fossil enamel. The observed IR bands (——), the Lorentzian components (– – –) and the fitted spectra (. . .).

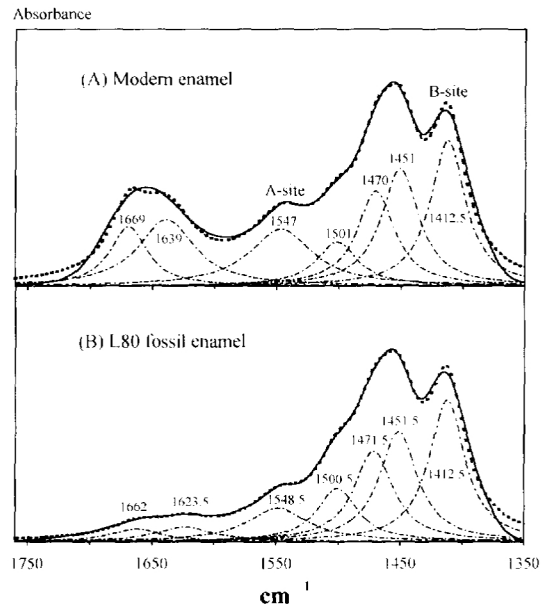

Fig. 4. ν_3 CO_3^{2-} bands of (A) the modern red deer enamel and (B) L80 fossil enamel. The observed IR bands (——), the Lorentzian components (– – –) and the fitted spectra (. . .).

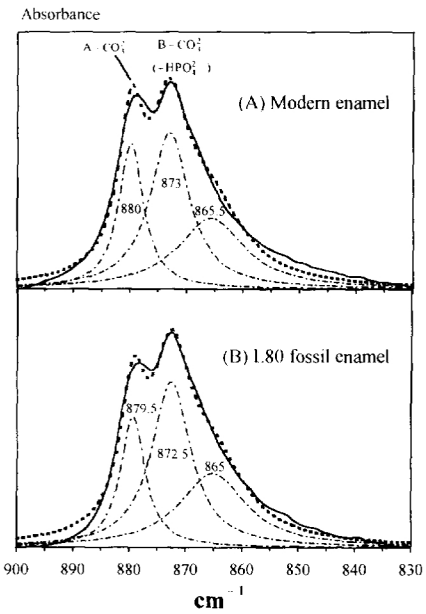

Fig. 5. ν_2 CO_3^{2-} bands of (A) the modern red deer enamel and (B) L80 fossil enamel. The observed IR bands (——), the Lorentzian components (– – –) and the fitted spectra (. . .).

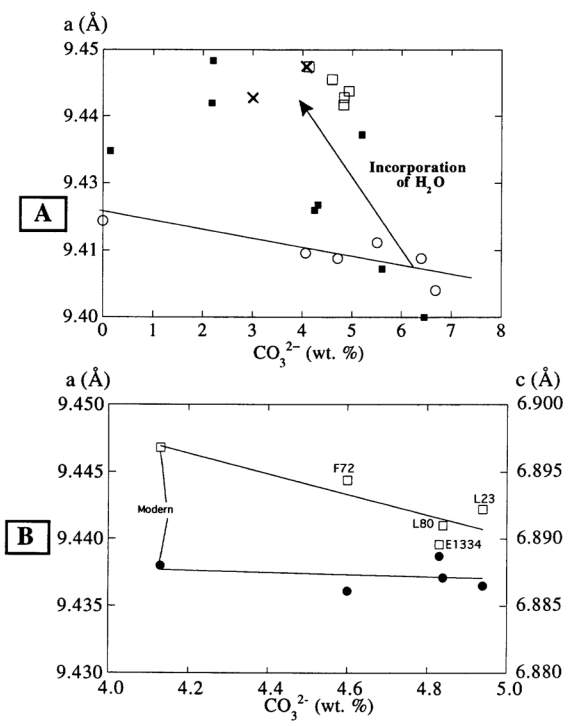

Fig. 7. (A) Variation of a lattice parameter with CO_3^{2-} content for synthetic apatites, human and red deer enamels; □: modern and fossil red deer enamel; ×: human enamel (Young and Mackie, 1980; Nelson and Featherstone, 1982); ■: synthetic "aqueous" apatites (Nelson and Featherstone, 1982; Okazaki, 1983); ○: synthetic "high temperature" apatites (Nelson and Featherstone, 1982). (B) Variation of a and c lattice parameters with CO_3^{2-} content for the modern and fossil red deer enamels; □: a parameter; ●: c parameter.

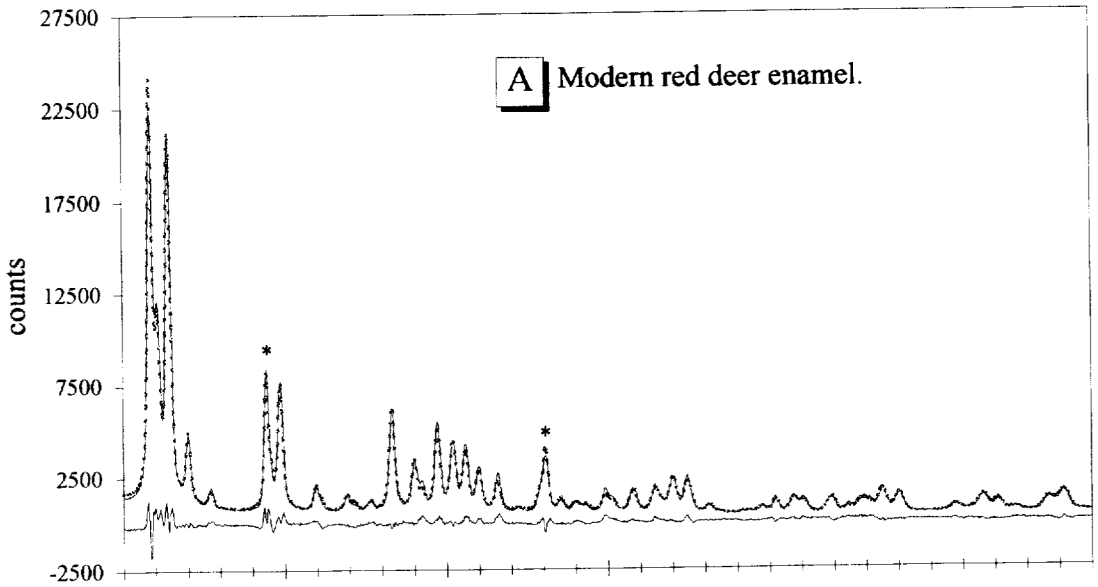

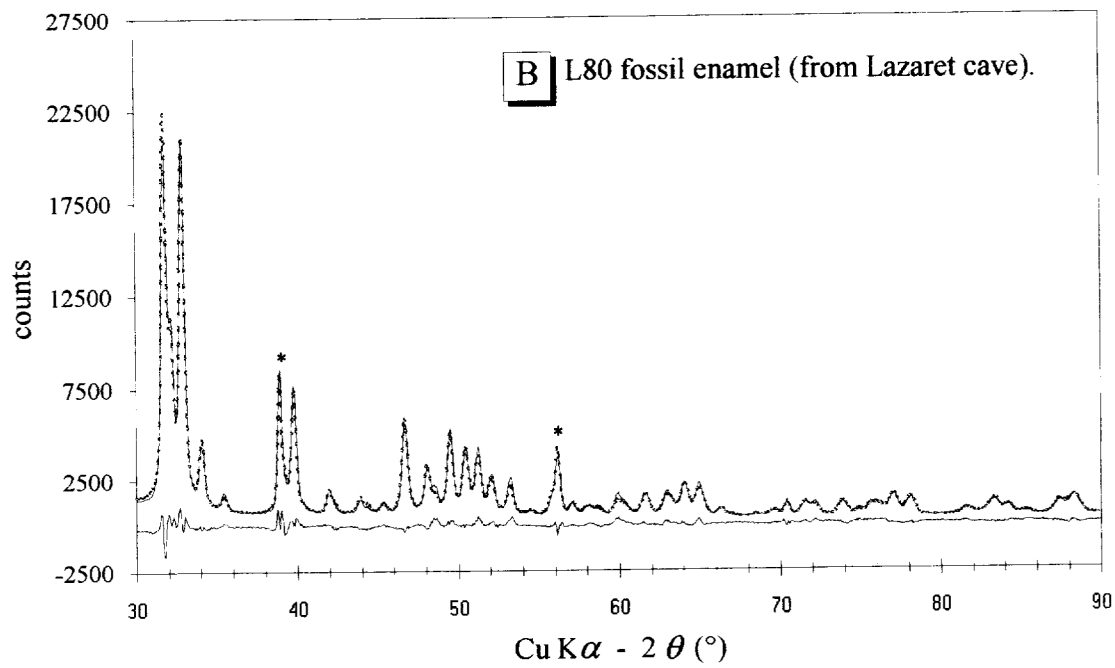

* NaF internal standard.

Fig. 6. X-ray powder diffraction patterns for (A) the modern red deer enamel and (B) L80 fossil red deer enamel. The observed pattern (——) and the calculated pattern (. . .). The bottom continuous line yields the difference between observed and calculated patterns.

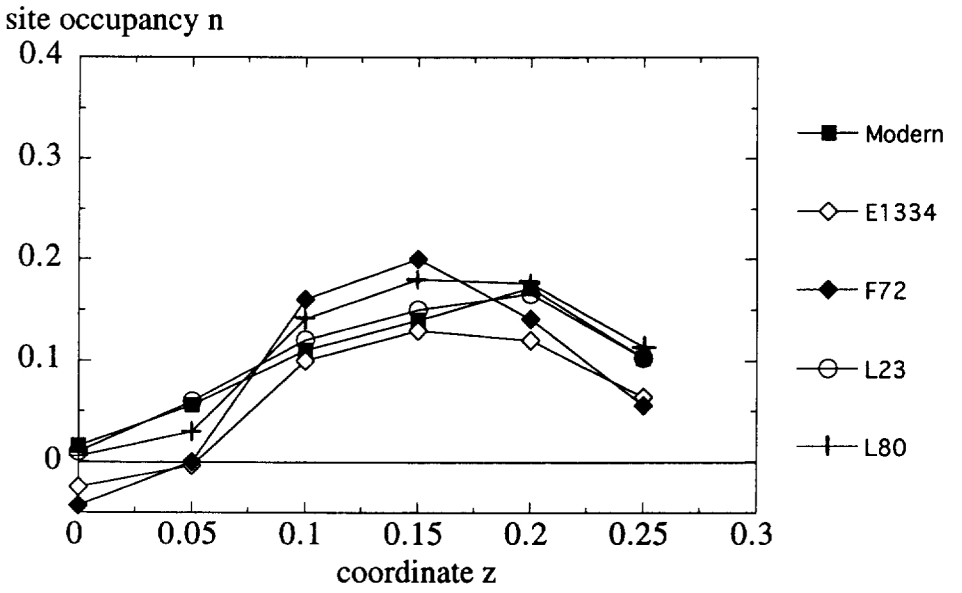

Fig. 8. Distribution of the apparent scattering density of the channels along the hexad 6_3 axis, refined for modern and fossil enamels.

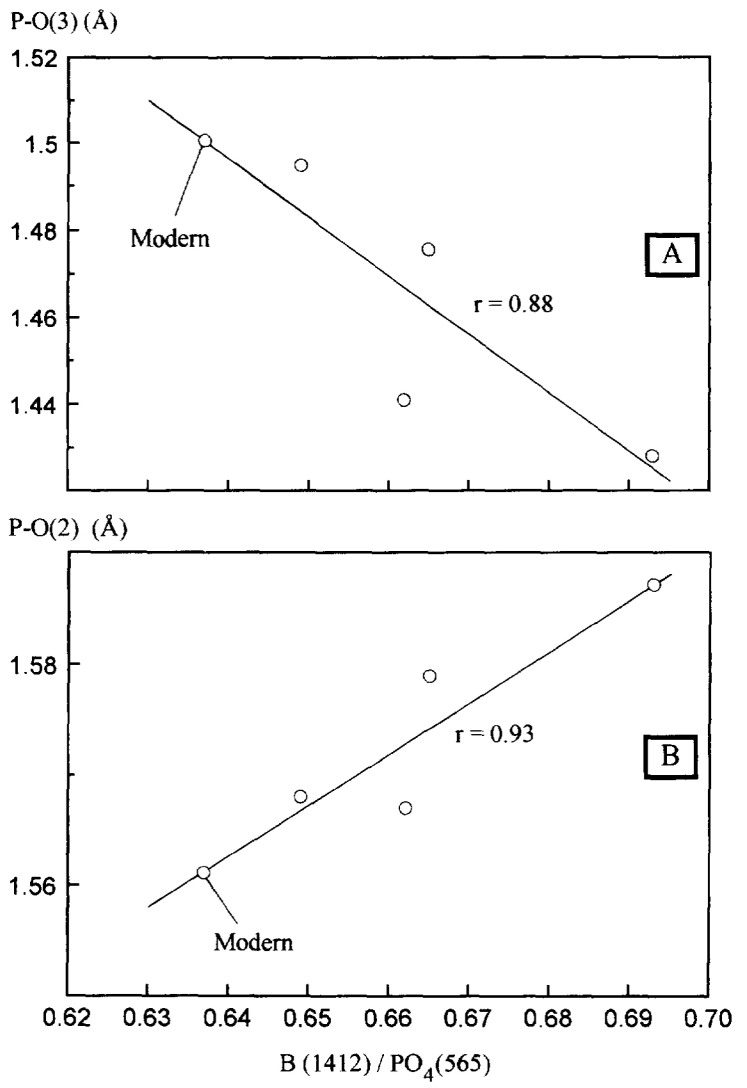

Fig. 9. Correlation between P–O distances and the carbonate contents as determined from the IR area band ratio B(1412)/PO_4(565). (A) P–O(3) distance (B) P–O(2) distance.

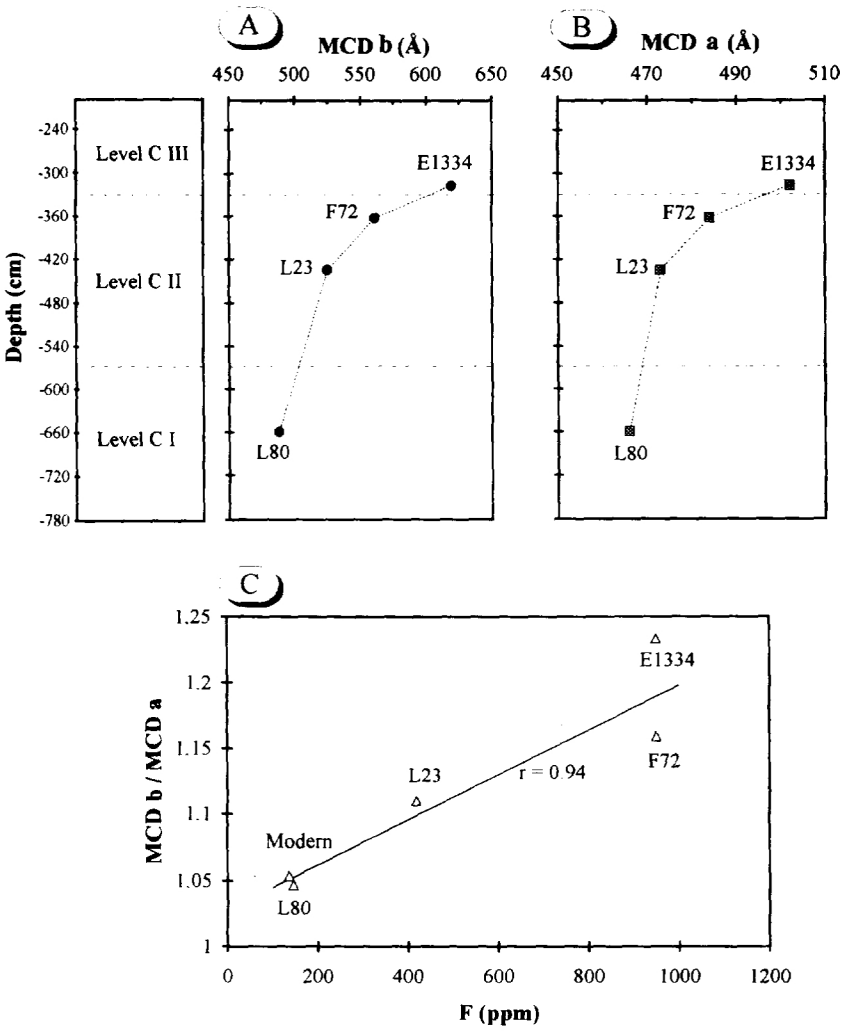

Fig. 10. Variation of mean coherent domain size (Å) along a and b directions *vs* depth for fossil red deer enamels (A) MCDb and (B) MCDa, respectively. (C) Correlation between MCDb/MCDa ratios and the contents for modern and fossil red deer enamels.

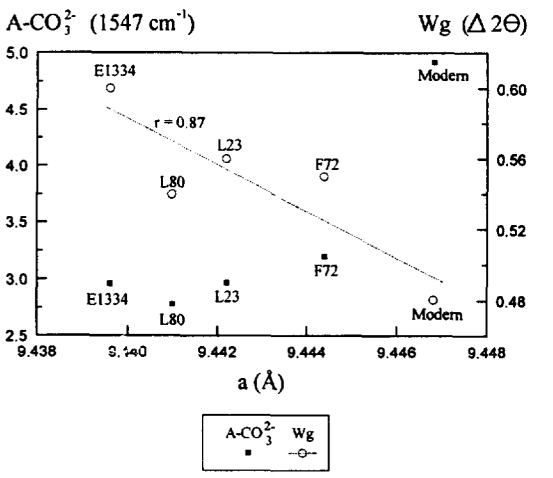

Fig. 11. Variation of *a* lattice parameter with CO_3^{2-} content at A-site (measured from 1547 cm^{-1} IR band area) and Wg (Δ2Θ) for modern and fossil red deer enamels; ○: Wg; ■: A-CO_3^{2-}.